Science of the Total Environment 810 (2022) 152193

Contents lists available at ScienceDirect

Science of the Total Environment

journal homepage: www.elsevier.com/locate/scitotenv

Thermal influences on groundwater in urban environments – A multivariate statistical analysis of the subsurface heat island effect in Munich

Fabian Böttcher *, Kai Zosseder

TUM - Technical University of Munich, Arcisstraße 21, 80333 Munich, Germany

HIGHLIGHTS

- Analysis of the subsurface urban heat island including anthropogenic and natural factors using large temperature datasets
- Identification of the dominant increasing and decreasing influences on the groundwater temperature
- Comparative analysis of the depth-dependent change in the magnitude of influences
- Introduction of a thermal exposure score to spatially assess thermal influences
- Seasonal adjustment of multi-temporal measurements by passive heat tracing

GRAPHICAL ABSTRACT

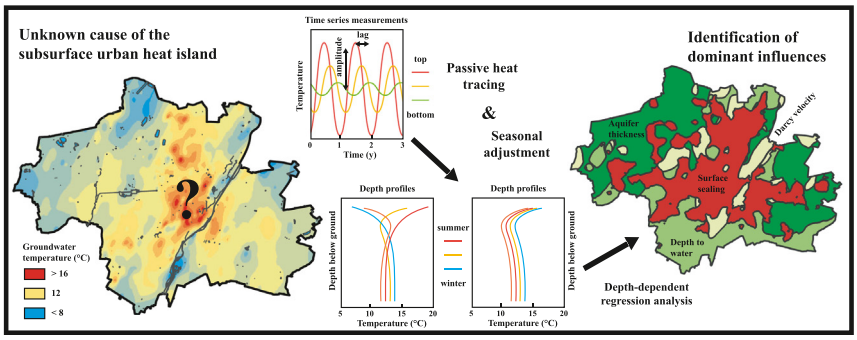

ARTICLE INFO

Article history:
Received 17 August 2021
Received in revised form 29 October 2021
Accepted 1 December 2021
Available online 7 December 2021

Editor: Christian Herrera

Keywords:
Groundwater temperature
Urban heat island
Temperature time series
Temperature-depth profile
Passive heat tracing

ABSTRACT

Shallow aquifers beneath cities are highly influenced by anthropogenic heat sources, resulting in the formation of extensive subsurface urban heat islands. In addition to anthropogenic factors, natural factors also influence the subsurface temperature. However, the effect of individual factors is difficult to capture due to high temporal dynamics in urban environments. Particularly in the case of shallow aquifers, seasonal temperature fluctuations often override the influence of existing heat sources or sinks. For the city of Munich, we identify the dominant anthropogenic and natural influences on groundwater temperature and analyse how the influences change with increasing depth in the subsurface. For this purpose, we use depth temperature profiles from 752 selected groundwater monitoring wells. Since the measurements were taken at different times, we developed a statistical approach to compensate for the different seasonal temperature influences using passive heat tracing. Further, we propose an indicator to spatially assess the thermal stress on the aquifer.

A multiple regression analysis of four natural and nine anthropogenic factors identified surface sealing as the strongest and the district heating grid as a weak but significant warming influence. The natural factors, aquifer thickness, depth-to-water and Darcy velocity show a significant cooling influence on the groundwater temperature. In addition, we show that local drivers, like thermal groundwater uses, surface waters and underground structures do not significantly contribute to the city-wide temperature distribution. The subsequent depth-dependent analysis revealed that the influence of aquifer thickness and depth-to-water increases with depth, whereas the influence of Darcy velocity decreases, and surface sealing and the heating grid remain relatively constant. In conclusion, this study shows that the most critical factor for the mitigation of future groundwater warming in cities is to minimize further sealing of the ground, to restore the permeability of heavily sealed areas and to retain open landscapes.

* Corresponding author.
E-mail address: fabian.boettcher@tum.de (F. Böttcher).

http://dx.doi.org/10.1016/j.scitotenv.2021.152193

1. Introduction

Cities are usually warmer than their rural surroundings (Oke, 1982). This phenomenon is known as the "urban heat island", and it is present in the atmosphere, on the surface and in the subsurface as the so-called *subsurface urban heat island* (SSUHI) (Gunawardhana et al., 2011; Oke et al., 2017). Thus, in cities with shallow aquifers, valuable groundwater resources are exposed to numerous anthropogenic impacts (Epting et al., 2013; Menberg et al., 2013a). Elevated temperatures can affect groundwater quality, microbial ecosystems or contaminant transport (Brielmann et al., 2009; Bonte et al., 2013; Jesußek et al., 2013; García-Gil et al., 2018). Furthermore, despite the influence on the resource itself, studies have highlighted the additional risk of drinking water quality degradation by elevated ground temperatures as water travels through the drinking water distribution system (Müller et al., 2014; Agudelo-Vera et al., 2020). Therefore, it is essential to gain deeper insights into how the different thermal sources and sinks affect subsurface and groundwater temperatures and support the development of adequate measures for the future protection of urban groundwater bodies (Ferguson and Woodbury, 2007; Eggleston and McCoy, 2015; Zhu et al., 2015; Benz et al., 2017; Epting et al., 2017).

While an increasing amount of SSUHI phenomena are described around the world (Taniguchi et al., 2005; Taniguchi et al., 2009; Yalcin and Yetemen, 2009; Lokoshchenko and Korneva, 2015; Bucci, 2017; Marschalko et al., 2018; Visser et al., 2020), studies have already identified a set of related anthropogenic heat sources (Menberg et al., 2013b). Primarily, heat loss from buildings and higher ground surface temperatures resulting from changed land use are held accountable for elevated subsurface temperatures (Ferguson and Woodbury, 2004; Reiter, 2007; Benz, 2018; Hemmerle et al., 2019). Furthermore, previous work successfully introduced methods to quantify anthropogenic heat fluxes through analytic calculations (Menberg et al., 2013a; Benz, 2015).

In addition, the groundwater temperature is a governing factor for the efficiency of thermal use. Thus, the SSUHI promotes and is also remediated by installing groundwater heat pumps (Allen et al., 2003; Zhu et al., 2010; Epting and Huggenberger, 2013; Rivera et al., 2017). In contrast, groundwater use for cooling is hampered, whereas the cooling demand in cities is likely to increase in the future (Li, 2019; van Ruijven et al., 2019). As a result, the controversial discussion about the growth of new groundwater cooling systems will benefit from a more precise understanding about the magnitude of thermal influences on large scale (Blum et al., 2010; Visser et al., 2020).

The thermal characterisation of shallow aquifers remains challenging because groundwater temperatures at depths of up to 10 m are influenced considerably by seasonal temperature variations on the surface (Banks, 2009; Stauffer et al., 2014; Farr et al., 2017). In shallow aquifers below urban areas, seasonal variations coincide with various anthropogenic heat sources, like for example sealed surfaces or subsurface building parts. This results in highly dynamic and complex thermal conditions, where identifying influencing heat sources is not straightforward (Ferguson and Woodbury, 2007; Taniguchi et al., 2007). In detail, single measurements within the seasonal fluctuation zone do not represent the undisturbed conditions required, e.g. the annual mean temperature, to link elevated ground temperatures to specific influences (Menberg et al., 2013b). To circumvent this problem, studies commonly rely on deeper measurements underneath the zone of seasonal variations (>15 m) to analyse the dependency between heat sources near the surface and groundwater temperatures (Benz et al., 2016; Benz, 2018; Hemmerle et al., 2019). Shallow aquifers have not been extensively studied despite their importance, e.g., for thermal use or water for domestic or industrial use. In addition, the interpretation of groundwater temperatures closer to the ground surface is potentially beneficial for revealing the impact of specific heat sources and detecting climate-induced short-term changes.

Previous research has largely been focused on evaluating the anthropogenic causes of the SSUHI effect. However, especially in hydraulically conductive gravel aquifers, it is assumed that the intensity of the SSUHI further depends on hydrogeological properties like the thickness of the saturated zone, depth-to-water or groundwater velocity (Epting et al., 2013; Bidarmaghz, 2019). Hence, a comparative analysis of hydrogeological and anthropogenic factors based on a large dataset of measurements can contribute to a deeper understanding of increasing and decreasing influences on groundwater temperatures and help to establish measures to mitigate increasing groundwater temperatures in cities.

The thermal conditions of Munich's quaternary aquifer were previously assessed and discussed by Dohr (1989, 2011), Dohr and Gruban (1999) and Zosseder (2013). As early as the first study, the anthropogenic heat influence was recognised and various sources were identified. During the construction of the subway, measurements in the surroundings of the tunnels revealed a considerable local temperature increase (1.0 °C – 2.0 °C) in the groundwater (Dohr, 1989). Spatially distributed measurements showed that temperatures gradually increase towards the city centre with locally cooler areas in parks (Dohr and Gruban, 1999). Thus, building density and surface sealing were assumed to play a significant role, whereas previous studies were unable to prove beyond doubt any relevant influence of the district heating grid, the sewerage or the infiltration systems. Strong local thermal influence is further attributed to the river *Isar* and large subsurface buildings which partially reach into the groundwater body.

With a more precise knowledge about the properties of the aquifer and its use, an influence of saturated groundwater thickness and large thermal uses for cooling became apparent (Böttcher et al., 2019; Albarrán-Ordás and Zosseder, 2020; Theel et al., 2020). However, these hypotheses were mainly tested by interpreting individual measurements and have never been analysed comparatively using all the historical and recent temperature datasets to gain quantitative statistical measurements about the intensity of all potential influences. Furthermore, temperature datasets with a vertical resolution, like the depth profile measurements used, have not been available before. As a result, previous studies had to rely on spatially interpolated measurements taken 1 m below the groundwater level and mainly lie within the zone of seasonal fluctuations (Dohr, 1989, 2011; Dohr and Gruban, 1999).

To tackle the shortcomings mentioned, we investigated the seasonal fluctuations in the shallow gravel aquifer of the city of Munich with a data basis of 71 multi-annual groundwater temperature time series. Subsequently, we estimated the mean thermal diffusivity with passive heat tracing and used the information derived on seasonal fluctuations to adjust a city-wide dataset of 752 vertical temperature profiles originating from different measurement times on one reference date to reproduce the same seasonal state. With this seasonally corrected dataset, we identified the dominant large-scale and local-scale drivers of the SSUHI effect by multiple linear regression. Finally, we analysed the depth-dependent measurements statistically to show vertical changes in the magnitude of the previously identified five dominant natural and anthropogenic influences.

The study presented in this paper assesses the natural and anthropogenic thermal influences on the shallow aquifer of Munich, proposes an approach to adjust the seasonal variation of temperature measurements to the same seasonal state and highlights the mitigating role of hydrogeological properties in the context of anthropogenic groundwater warming.

2. Materials and methods

2.1. Climatic and hydrogeological overview of the study site

The city of Munich lies in the south of Germany, about 50 km north of the Alps. With over 1.5 million inhabitants, it is the most densely populated city and one of the fastest-growing municipalities in Germany. Munich has a warm-summer humid continental climate with a mean annual precipitation of approx. 950 mm (1977–2000) and a mean air temperature of 9.5 °C (1955–2018) (Peel et al., 2007; Mühlbacher, 2020). The city's air temperature shows a significant upward trend of 0.31 °C per decade over the reference period (1955–2018). In line with this observation, a decrease in the number of frost days with air temperatures below freezing and an increase in the number of summer days with a maximum temperature of at least 25 °C was recognised in the long-term trends. The occurrence of summer days rose from 28 in 1955 to 60 in 2018 and frost days declined from 95 in 1955 to 68 in 2018. Measurements by the German Weather Service

also show that the city's nightly air temperatures are on average 1.7 K higher than the nearby rural areas (Mühlbacher, 2020). Due to its green spaces and large parks, no continuous heat island forms over the entire city (cf. Fig. 1e). Elongated areas, like the north-south oriented bed of the river Isar, contribute largely as pathways for the flow of cold air into the city. Thus, the heat island of Munich is compartmentalised and subject to a great number of local and regional exchange processes (Funk et al., 2014). This situation is certainly reflected in the subsurface.

The city lies at a mean altitude of 519 m above sea level (m.a.s.l.) on the so-called Munich Gravel Plain, which dips northwards by about 0.5%. Its present shape evolved primarily during the Pleistocene period when large amounts of fluvioglacial sandy gravel were deposited on the former

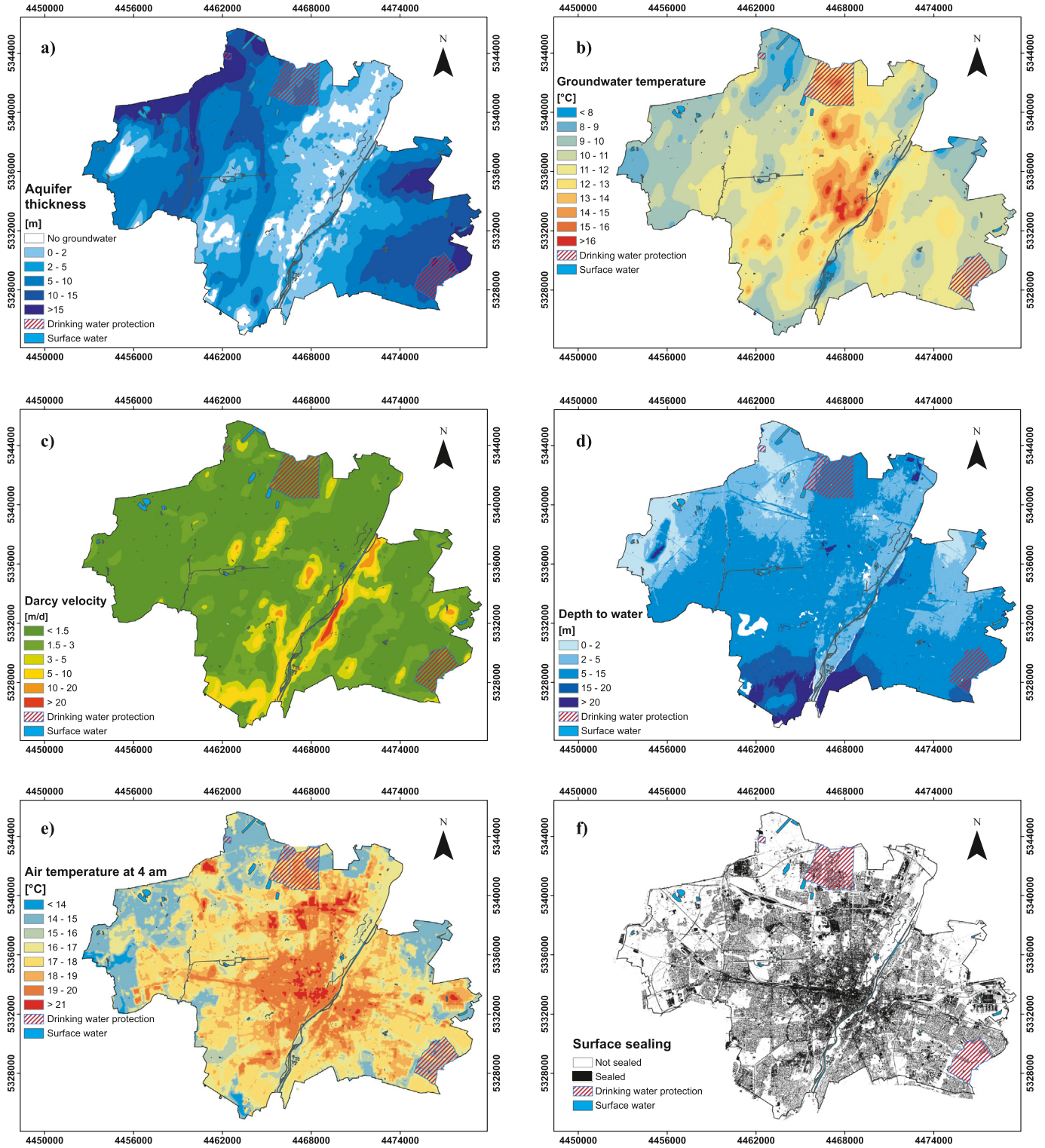

Fig. 1. City-wide datasets of a) saturated aquifer thickness of the quaternary groundwater, b) groundwater temperature measured in April 2014 one metre below groundwater level, c) Darcy velocity, d) depth-to-groundwater, e) Modelled air temperature 2 m above ground at 4 am in summer adapted from Funk et al. (2014) and f) surface sealing (cf. Section 2.2.3).

Tertiary landscape (Jerz, 1993). Due to the past drainage system, the morphology of the Tertiary surface is characterised by an uneven relief of channels and ridges (Kerl et al., 2012; Albarrán-Ordás and Zosseder, 2020). The limno-fluviatile Tertiary sediments are mainly composed of fine sand with a varying silt content intersected by silt and clay layers (Lemcke, 1988). In comparison with the overlying gravels, the hydraulic conductivity of the Tertiary layers is generally two to five orders of magnitude lower and, consequently, the Tertiary sediments mostly confine the quaternary groundwater towards the bottom (Jerz, 1993; Zosseder, 2007). As a result, Fig. 1a shows that the saturated thickness of the quaternary aquifer, derived from mean low water conditions, varies largely throughout the city area with a 1st quartile of 2.5 m and a 3rd quartile of 10.2 m (Albarrán-Ordás and Zosseder, 2020; Theel et al., 2020). In general, the gravel sediments form a productive aquifer with an average hydraulic conductivity of 3.7×10^{-3} m/s based on the hydrofacies types occurring (Theel et al., 2020). As displayed in Fig. 1c and d, a high average Darcy velocity with a mean of 1.8 m/d (1st qu. 0.8/3rd qu. 1.9) and a low depth-to-water provide favourable conditions for thermal use in open-loop systems (Böttcher et al., 2019). The low depth-to-water, which decreases towards the north, commonly lies in depths from 4 m (1st qu.) to 10 m (3rd qu.) and, therefore, large parts of the groundwater body are exposed to seasonal temperature variations. Assuming 15 m as a hypothetical threshold for significant seasonal temperature oscillations, the groundwater in 91% of the city's area is subject to those influences (Banks, 2012). In consequence, a periodical seasonal variation is present in most temperature measurements and complicates temporal or spatial interpretation.

2.2. Groundwater and infrastructure datasets

The following sections present the available groundwater and urban infrastructure datasets. In detail, depth profile and time-series measurements are distinguished to analyse specific vertical, temporal and lateral influences. Furthermore, the spatial datasets of the potential natural or anthropogenic thermal influences are introduced. A summary description of all datasets can be found in Table 1, and Fig. 2 summarises the spatial distribution of the temperature measurements in the city.

2.2.1. Temperature depth profiles

From 2012 to 2017 in the months April to June, we measured groundwater temperatures in periodical field campaigns every metre below ground level (mbgl) in the water columns of 752 selected monitoring wells throughout the city (cf. Fig. 2). In general, most of the approximately 16,000 measurements were taken at shallow depths of 2 to 20 mbgl. Although the measurements are available in a relatively short period from April to June, seasonal temperature fluctuations are already apparent. In Fig. 3a, distributions of measurements for each month and metre below ground are displayed as boxplots. From April to June, the mean temperature at 2 mbgl already deviates by 3.7 °C. The influence is still visible up to 6 mbgl. April is the most frequently measured month, with an average of 193 measurements, followed by June with 159 and May with 116.

2.2.2. Time series measurements

In Munich, 71 multi-annual time-series taken at a known constant depth are available (cf. Fig. 2). The city's water authorities have recorded the longest 19 series at a 4-week frequency by hand measurements since 2009. Nine additional wells have been equipped with data loggers by the city's energy supplier in 2011, recording at a two-hour frequency since that time. The energy supplier extended this monitoring programme in 2014 with six data loggers, in 2015 with two, in 2016 with two, in 2017 with eight and in 2018 with another three. All data loggers that are maintained by the energy supplier were added at new sites and are equipped with NTC 30 temperature sensors. Furthermore, the city's water authorities started an extensive automated monitoring programme in 2018 by installing 20 additional data loggers at new sites that record hourly values with NTC 30 temperature sensors. The German Weather Service (DWD) also maintains one soil temperature monitoring station in the city, which records at five depths of up to 1 m on an hourly basis with PT 100 temperature sensors, since July 1997. Since the measurements are not conducted within an integrated monitoring network, the selection of sites does not follow a common strategy. A situation that is often found in large cities.

2.2.3. Spatial hydrogeological datasets

In the Munich Gravel Plain, high-resolution spatial datasets of hydrogeological properties provide the opportunity to analyse their influences on groundwater temperature in detail. Within a four-year project, funded by the Bavarian Environmental Agency (LfU), the Chair of Hydrogeology elaborated the surface of the quaternary aquifer basis of the entire Munich Gravel Plain based on the interpretation of over 48,000 borehole logs. In addition, an extensive reference date measurement was carried out in April 2014, capturing the hydraulic dynamics during mean low groundwater conditions (Böttcher et al., 2019; Albarrán-Ordás and Zosseder, 2020). The conditions represent an equilibrated and robust flow field that reflects the common hydraulic situation throughout the year. A comparison with other available groundwater table maps from the past, including datasets with less sample points and thus, lower accuracy, showed only minor local changes in the groundwater flow field. Hence, the dataset has a high general validity and only minor errors are introduced in derived datasets. Throughout the entire Munich Gravel Plain, over 6000 hydraulic head measurements were used to interpolate a map of the groundwater table by variogram analysis and block kriging (Böttcher et al., 2019; Albarrán-Ordás and Zosseder, 2020). The saturated thickness of the aquifer was derived by subtracting the surface of the aquifer basis from the interpolated hydraulic head (cf. Fig. 1a and Fig. 2). The hydraulic head is further used to calculate the hydraulic gradient, and with the 2-m digital elevation model, the depth-to-water is computed (cf. Fig. 1d). During the 2014 field campaign, groundwater temperatures were measured one metre below groundwater level and one metre above total

Table 1
Feature count or spatial resolution and data type of the analysed datasets.

Spatial dataset	Count / Res.	Type	Dataset owner
Temperature depth profiles	752	Points	Chair of Hydrogeology (TUM)
Multi-annual temperature time series	71 / hourly to weekly	Points	Energy supplier / City of Munich
Saturated groundwater thickness	2 m	Raster grid	Bavarian Environmental Agency
Depth-to-water	2 m	Raster grid	Bavarian Environmental Agency
Darcy velocity	2 m	Raster grid	Bavarian Environmental Agency
Cooling systems (injection wells)	376	Points	Bavarian Environmental Agency
Heating systems (injection wells)	2341	Points	Bavarian Environmental Agency
Surface waters with groundwater-interaction	12	Polygons	OpenStreetMap contributors (2021)
Surface sealing	0.5 m	Raster grid	German Aerospace Centre
Built-up area	2 m	Raster grid	OpenStreetMap contributors (2021)
Sewer system sections	14783	Line segments	City of Munich
Heating grid sections	9663	Line segments	Energy supplier
Deep buildings	1286	Polygons	City of Munich
Metro stations	96	Polygons	City of Munich
Tunnel sections	127	Line segments	City of Munich

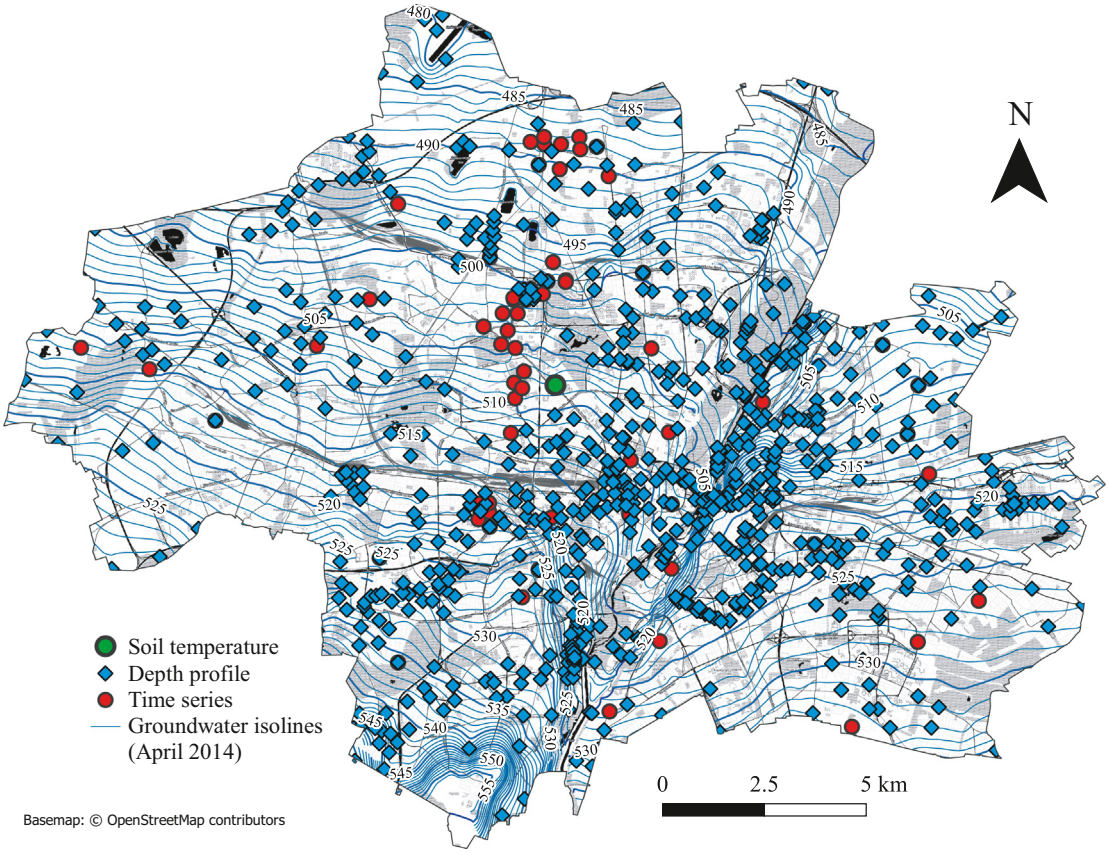

Fig. 2. The spatial distribution of the different temperature datasets within the study area Munich and the interpolated groundwater isolines with hydraulic head labels from the reference date measurement in April 2014.

depth in around 1800 observation wells, and a temperature distribution map was interpolated by block kriging for the entire gravel plain (cf. Fig. 1b).

The Darcy velocity was calculated by multiplying the interpolated hydraulic conductivity map of Theel et al. (2020) with the hydraulic gradient and therefore, the Darcy velocity incorporates the uncertainties of those two dataset (cf. Figs. 1c and 2). As stated above, we assume minor errors from hydraulic gradients. The hydraulic conductivity, however, can be heterogeneous at small scale and the distribution of analysed pumping tests is still not sufficient to capture this heterogeneity (Theel et al., 2020). The used 542 pumping tests represent the entire data currently available and thus, this residual uncertainty has to be taken into account in further interpretations.

2.2.4. Spatial infrastructure dataset

In the present study, surface sealing is used as the primary dataset to reflect urbanization and anthropogenic land use (cf. Fig. 1f). The German Aerospace Centre (DLR) conducted the mapping with a mosaic of eight-

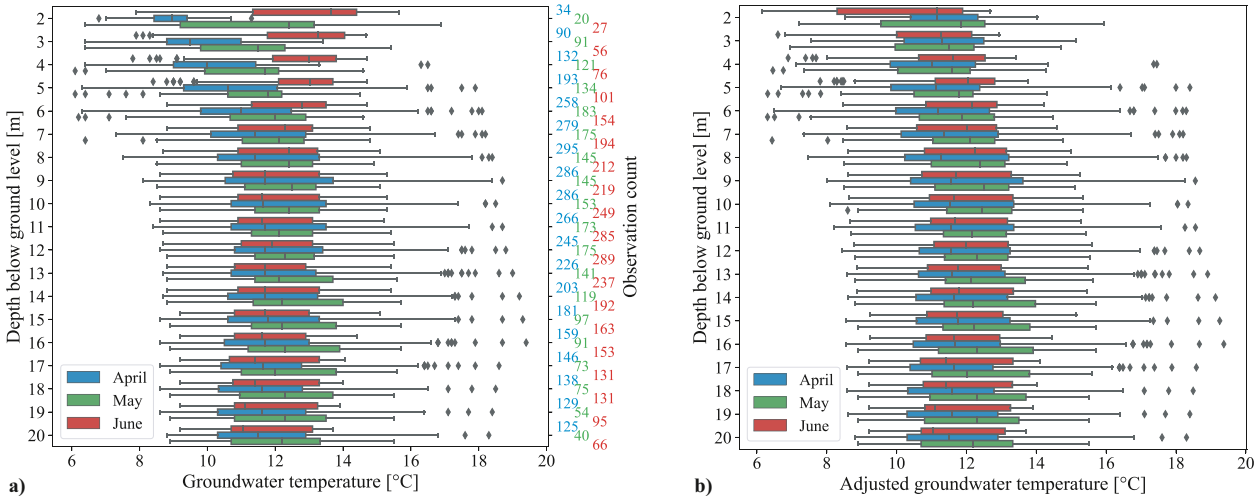

Fig. 3. Monthly distribution of a) the initial groundwater temperatures and b) the seasonally corrected temperatures that are referenced to the 12th of May in a one-metre vertical resolution displayed as boxplots with an interquartile range (IQR) of 50% and whiskers with 1.5*IQR. The right-hand y-axis of a) shows the observation count per depth below ground in the colour of the respective month.

band image data at a spatial resolution of 2 m from the WorldView-2 sensor, recorded on the 12th of July and the 2nd of October 2011 (Leichtle et al., 2018). The binary classification of the multispectral satellite imagery is performed by a semi-automatic object-based approach, which integrates auxiliary vector datasets, like building boundaries from the German Official Topographic Cartographic Information System (ATKIS), on different evaluation levels (Wurm et al., 2011).

In addition to the spatial grid information, also vector datasets of potential anthropogenic heat sources are evaluated. As an extension to the analysis of surface sealing, we include building outlines (OpenStreetMap contributors, 2021). Furthermore, we considered deep building basements that reach into the groundwater body, metro stations and surface waters separately as polygon features. As line features, the district heating grid, the sewer system and tunnels are included in the analyses. Finally, thermal uses for heating and cooling purposes are characterised as point features. These datasets were provided by the City of Munich and the Munich Public Services SWM GmbH (cf. Table 1).

2.3. Correction of depth profile temperatures

Surface temperature oscillations attenuate naturally in the ground, while the lag of the signal increases and the amplitude decreases with depth (Banks, 2009). Diurnal variations only reach several decimetres into the ground, whereas the boxplots in Fig. 3a already show that substantial seasonal variations penetrate a few metres into the ground until the signal dissipates (Van Wijk and de Vries, 1963). As outlined in the introduction, this variation impedes identifying additional anthropogenic or natural influences on the ground temperature. Therefore, the following section covers the developed approach of estimating the seasonal variation present in the study area. The depth-depended seasonal oscillation is further used to adjust the multi-temporal depth profile dataset to one reference date. The adjustment enables the comparison of temperatures that had originally been measured at different times within the zone of seasonal fluctuation. As a result, the adjusted temperatures can be used in regression analyses to reveal the influence of anthropogenic or natural heat sources (cf. Table 1).

The calculation of the typical seasonal variation is performed by estimating the thermal diffusivity through the extraction of amplitude and phase from the time-series data presented in Section 2.2.2. Initially, an additive decomposition into trend, seasonal and random components was carried out to calculate the amplitude of the seasonal oscillation (Kendall et al., 1983). First, the trend component was determined using a moving average as a low-pass filter with a symmetric window and equal weights. Then, the trend is removed from the time series, and the seasonal component is computed by averaging, for each time unit, over all periods. Finally, the error component is determined by removing the trend and the seasonal component from the original time series.

The seasonal components extracted from the differently deep time series, as shown in Fig. 4, (cf. Section 2.2.2) were further used to compute the cross-correlation between the shallowest time series and the deeper groundwater temperature time series (Venables and Ripley, 2002). As a result, the maximum cross-correlation determines the time lag between the respective groundwater temperature oscillations and the shallowest temperature oscillation, i.e. the ground temperature 1 m below surface. The amplitude and time lag data derived is then used to estimate the thermal diffusivity.

To describe an average thermal response in the groundwater, we assume no vertical fluid flow. Hence, the vertical heat transport is considered entirely conductive, and we assume that the seasonal influence is the only oscillation in the monitored depths (Goto, 2005; Hatch et al., 2006; Keery et al., 2007; Molina-Giraldo et al., 2011). Therefore, in a semi-infinite solid where the surface temperature is a harmonic function in time, the temperature fluctuation in time and depth $\Delta T(t,z)$ can be calculated by the initial amplitude at the surface (A), the thermal diffusivity (κ), the relative phase (θ) and the period of the oscillation (P) with (Stallman, 1965; Carslow et al., 1986)

$$\Delta T(t,z) = A\, e^{-z\sqrt{\frac{\pi}{\kappa P}}} \cos\left(\frac{2\pi t}{P} - \theta - z\sqrt{\frac{\pi}{\kappa P}}\right) \tag{1}$$

Thus, the damping of the amplitude (A_D) at a specific depth (z) can be calculated by an annual period of 365 days with

$$A_D = A\, e^{-z\sqrt{\frac{\pi}{\kappa P}}} \tag{2}$$

The progressive lag, as the relative phase difference ($\Delta\theta$) between a pair of temperature time series at different depths, is given by

$$\Delta\theta = \theta - z\sqrt{\frac{\pi}{\kappa P}} \tag{3}$$

which can be converted to a time lag (Δt) with

$$\Delta t = \frac{P}{2\pi}\,\Delta\theta \tag{4}$$

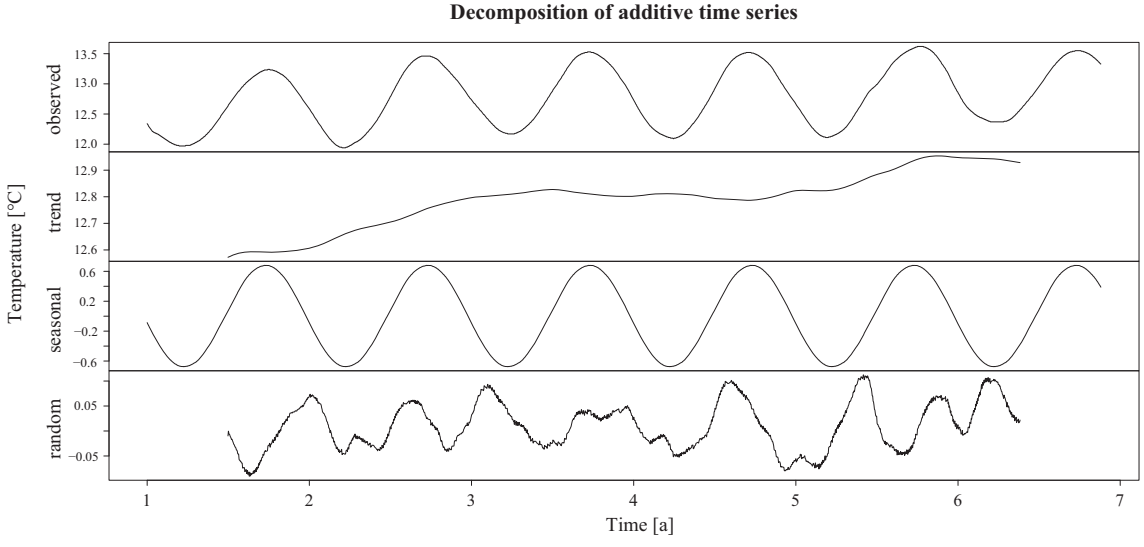

Fig. 4. Exemplary decomposition of a groundwater temperature time series with a seven-year duration and negligible residual random noise used to extract the seasonal component.

In consequence, the thermal diffusivity can be independently estimated, either from Eqs. (2) or (3) (Thomson, 1861). This is done by fitting the equations through a linear regression analysis using the extracted amplitude and time lag data of the recorded temperature time series with the specific measurement depths. The weighted arithmetic mean thermal diffusivity of the two estimates from the time lag and amplitude regression is then inserted in Eq. (1) for a time and depth-dependent calculation of the mean temperature change due to seasonal oscillation in the study area. To derive the weighted mean, weights are given by the reciprocal of the regression coefficient's variance.

Furthermore, Eq. (1) can be applied to the multi-temporal depth profile dataset to derive the seasonal temperature difference $\Delta T(t_0, z)$ originating from different measurement dates and depths. Thus, a corrected temperature (T_0) is calculated by adjusting all the original temperature values (T) to a single measurement time through

$$T_0 = T + \Delta T(t_0, z) - \Delta T(t, z) \quad (5)$$

With this, the difference of the seasonal temperature share (ΔT) at the desired time (t_0) and the actual measurement time (t) is calculated. After subtracting the seasonal share from the temperature measurements, the adjusted temperature dataset is used to evaluate the driving and diminishing factors on the SSUHI.

2.4. Statistical analysis of thermal influences on the groundwater

This section describes the procedures that we apply to account for the structurally different impact of several factors. Following Visser et al. (2020), we distinguish between large-scale factors and local-scale factors.

For large-scale factors, i.e., the raster grid datasets summarised in Table 1, we initially determine the area that shows the strongest correlation with the measured groundwater temperatures. Since the thermal influence on a well arises primarily from up-gradient in an advection-dominated aquifer, it is relevant to query the area where dispersive effects have not yet dispelled the dependency between the respective spatial factor and the groundwater temperature. Hence, we derive the maximum Pearson correlation by varying the extent of the up-gradient area in which the spatial factor is aggregated. Specifically, the mean value within an up-gradient directed triangle is computed for all well locations, as shown in Fig. 5a. This aggregation is repeated with a combination of opening angles at the well and up-gradient triangle lengths. Subsequently, the correlation of the aggregated factor values is conducted with the seasonally adjusted mean temperature per depth profile. The resulting correlation matrix for surface sealing is visualised in Fig. 5b as an example. The correlation reaches a maximum for triangles with a 60° opening angle and a length of 900 m. As a result, the strongest correlation of every large-scale factor is determined in a data-driven and exploratory manner. For the ratio of built-up area, the maximum correlation is present for a triangle with a 90° angle and a length of 1000 m. The angle and triangle length result for saturated aquifer thickness is 45°/1000 m, for Darcy velocity 120°/1400 m and for depth-to-water 30°/1400 m. The large triangle sizes for hydrogeological factors improve the robustness of the aggregated mean values, because generally the underlying values, like Darcy velocity, show less temporal and spatial variance in larger areas.

Local-scale influences, which are represented as geometrical features, behave differently (see Table 1). They potentially induce a thermal anomaly that diminishes while propagating down-gradient. Thus, we derive the distance from a local feature to a down-gradient observation well along the path of advection in the flow field (Konikow and Bredehoeft, 1984). In detail, we apply the implementation by Tauxe (1994) that allows the computation of a particle track from a point source by using the grid data of Darcy velocity and groundwater flow direction. In addition, we consider transversal dispersion in a simplified manner by excluding down-gradient connections if the well lies outside the study area's typical opening angle of a potential thermal plume of 15° (see Fig. 5c). Through this procedure, each observation well is attributed with its distances to all up-gradient local-scale factors, if present.

Finally, the influence of all factors is compared by estimating the standardized (beta-)coefficients in multiple linear regressions (Greenland et al., 1991; Schielzeth, 2010). In the following analyses of this study, we use beta-coefficients as an indicator for the comparative influence of a predictor with respect to the remaining predictors. For an estimation of beta-coefficients, the underlying data of the predictor variables was standardized by computing the z-score before performing the regression analysis (Menard, 2004; Everitt and Hothorn, 2011). As dependent variable, the adjusted mean temperature per depth profile is used for an initial evaluation of the overall influence and significance among all predictors (cf. Fig. 3b). Subsequently, only the dominant and significant predictors are used for computing the beta-coefficients each metre below ground from 3 to 20 m to reveal the depth-dependent change of influences.

Furthermore, the dominant large-scale factors are used to derive a map showing the aggregated heating and cooling influence on the groundwater by a specifically calculated thermal exposure score. Therefore, the beta-coefficients at the respective average depth of the groundwater body are used to solve the regression function with the z-score of the predictor's grid values. The resulting values are then normalised from −1 to 1 and

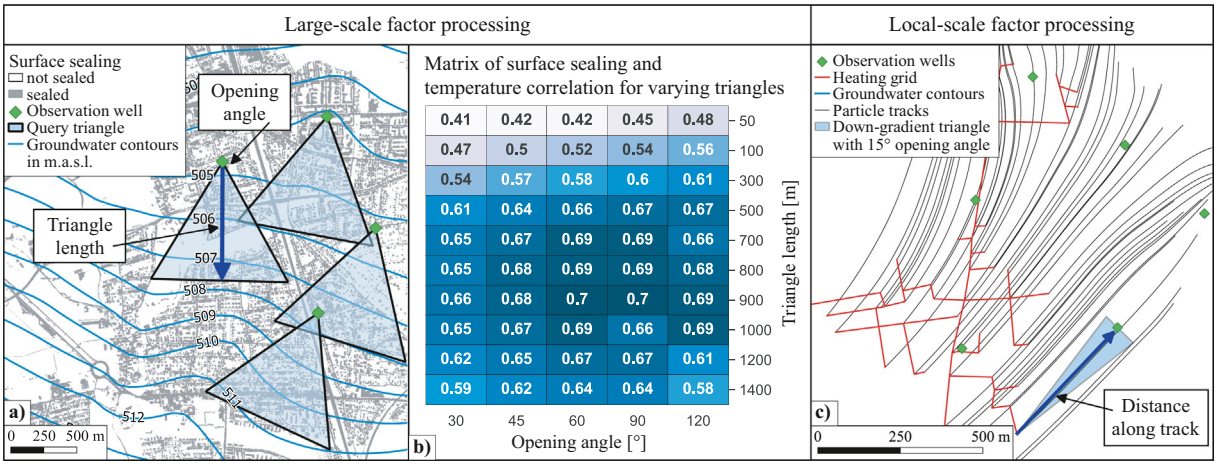

Fig. 5. a) Spatial evaluation of large-scale factors, i.e. raster grid data, with a calculation of the mean for different triangle sizes, b) resulting correlation matrix to identify the triangle size with the maximum correlation between the temperatures and the mean values with high correlation in dark blue and low correlation in light blue and c) particle track calculation for local-scale factors, i.e. vector data, to acquire the upstream distance between an observation well and a vector feature within a hypothetical plume of 15° opening angle.

offer a spatial visualisation of the comparative impact on the aquifer's thermal conditions. As a result, negative scores indicate areas where the urban and natural conditions have a cooling potential and positive values highlight areas where the groundwater likely to be heated by the assessed influences.

3. Results

In the following, results are presented in two sections. The first section comprises the seasonal variability analysis of the time-series data, the estimation of the weighted mean thermal diffusivity and the seasonal correction of the multi-temporal depth profile measurements to one reference date. The second section contains the comparative analysis of the potential influences of large and local-scale factors on groundwater temperature, the evaluation of vertical changes in the effect size of dominant influences and finally, the spatial assessment of the dominant city-wide influences, which is displayed in a thermal exposure map of the study area.

3.1. Seasonal temperature influences

Initially, the additive decomposition and cross-correlation of the seasonal component is conducted for all 71 groundwater temperature time series (cf. Fig. 4). With this, the amplitude of the seasonal variation and the time lag with respect to the shallowest measurement depth is obtained (cf. Section 2.4). The previous assumption of seasonality being the only relevant oscillation is proven by a constantly low residual variation in the random component. No diurnal or other substantial oscillations of lower frequency have been observed. The mean variance of the random component in the entire dataset is 0.07 °C, corresponding to only 4.3% of the mean seasonal variation. In addition, we reviewed, if general trends in the amplitudes are present. A negative trend in amplitudes would generally result in a positive correlation between seasonal and random component in the first half of the time series and a negative correlation in the second half. Four time series with a negative amplitude and five time series with a positive amplitude trend were identified. However, the identified time series are no influential outliers in the regression analyses and thus, do not negatively affect the thermal diffusivity estimation. Fig. 6a displays the derived seasonal time lags at the respective measurement depth. Subsequently, the data is used to fit Eq. (3) with the origin at one metre below ground, which results in a thermal diffusivity of $1.6 \times 10^{-6}\, m^2 s^{-1}$ with a standard error of $1 \times 10^{-7}\, m^2 s^{-1}$. The linear function fitted shows that a time lag of 14.4 days for every metre deeper below ground level can be expected as a mean value within the study area. As described in Section 2.4, the procedure of thermal diffusivity estimation is repeated using the seasonal amplitudes. Fig. 6b shows the measurement depth against the seasonal amplitude for the same time series data. Here, Eq. (2) is used to fit the two regression coefficients, which leads to an estimated thermal diffusivity of $1.1 \times 10^{-6}\, m^2 s^{-1}$ with a standard error of $1 \times 10^{-7}\, m^2 s^{-1}$.

From both thermal diffusivity estimations, the resulting weighted mean of $1.2 \times 10^{-6}\, m^2 s^{-1}$ with a standard error of $1 \times 10^{-7}\, m^2 s^{-1}$ is used in Eq. (1) to calculate the typical seasonal temperature oscillation of the study area from 0 mbgl to 20 mbgl. The mean temperature of 12.2 °C from the 1st of August 1997 to the 1st of August 2020 of the continuous measurements 1 mbgl of the DWD is added to obtain the monthly variation of one year.

With Eq. (5), all the depth-oriented temperatures are seasonally corrected by computing the temperature difference from the actual measurement date to the mean measurement date, i.e. the 12th of May, and adding this change to the initially measured value. In comparison with Fig. 3a, b displays the achieved absence of seasonal variation, especially observable from the mean values in the boxplots of the upper five metres. In detail, the variance two metres below the surface was reduced from 6.6 °C to 3.6 °C. Thus, the direct statistical analysis of measurements taken at different times is possible because the bias from changing seasonal conditions is marginalised. In the following, the adjusted temperature-depth profiles are used in multiple linear regression analysis to identify the dominant increasing and decreasing effects on the SSUHI.

3.2. Anthropogenic and natural influences on Munich's groundwater temperature

Following the approach described in Section 2.4, the correlations between groundwater temperature and the influential factors and cross-correlations among influential factors are determined. The resulting correlation coefficients between temperature and the respective factors are given in the first row of the matrix in Fig. 7. We observe equally strong positive correlations for sealed surfaces and built-up areas with high groundwater temperatures. They are followed by weaker positive correlations of the district heating grid and the Darcy velocity. In contrast, a weak negative correlation can be observed for the depth-to-water and the strongest negative correlation for saturated thickness. In general, the correlations of the factors with the temperature already give an initial indication of dependencies. However, only one factor at a time is considered while the superposition of all other factors are omitted. This can lead to significant biases, as can be observed for the Darcy velocity. The hypothesis is that dispersion increases with increasing flow velocity and thermal anomalies dissipate more quickly. Therefore, one would expect a cooling influence to be more

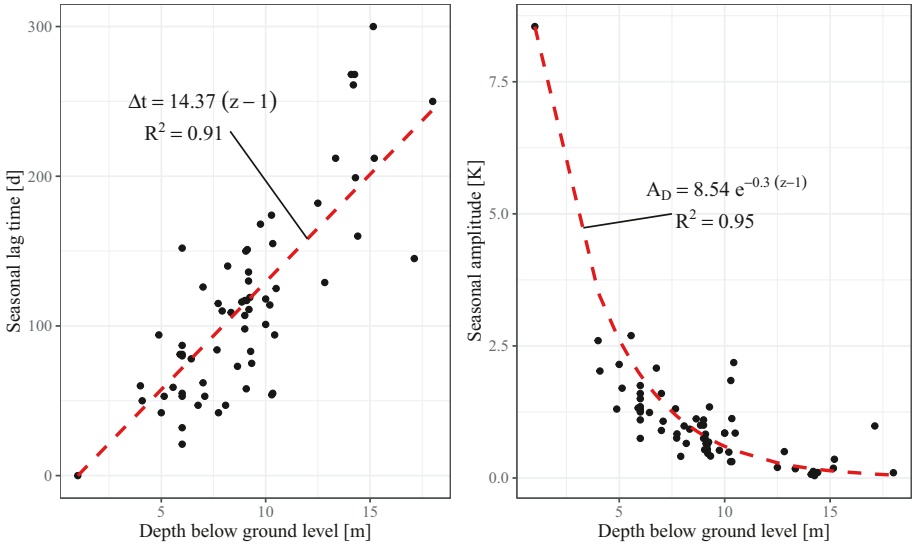

Fig. 6. a) Lag time and b) seasonal amplitude against depth below ground, both with the estimated regression function (dashed line), as well as the formula and R^2.

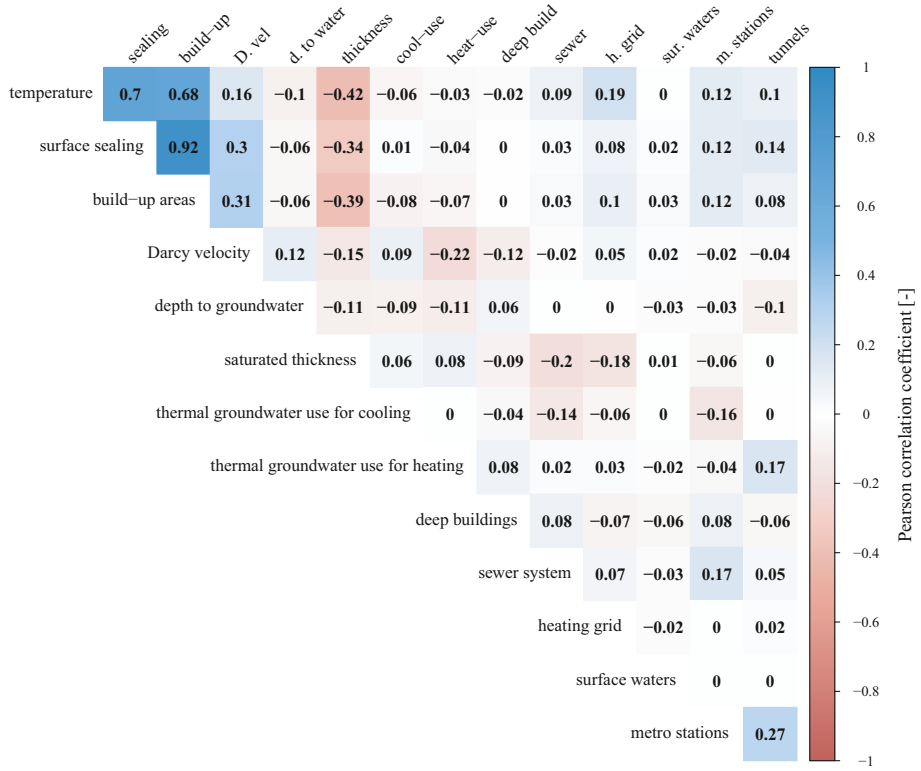

Fig. 7. Matrix of (Pearson-) correlations between predictors and the groundwater temperature in the first row and predictor correlations with colour coded correlation coefficients.

likely than a heating one. In the specific case of Darcy velocity, however, we also see a positive correlation with surface sealing and, simultaneously, a negative correlation with aquifer thickness. Since surface sealing has the strongest positive and aquifer thickness the strongest negative correlation with the temperature, the correlation of the Darcy velocity will be biased towards positive values. This result shows that a comparative analysis in a multiple regression is necessary to further reveal the heating and cooling effects on the groundwater without considerable bias.

Apart from the correlation with groundwater temperature, Fig. 7 shows the cross-correlation among all predictors. A very large positive correlation of surface sealing with built-up area indicates the presence of multicollinearity. The magnitude of multicollinearity in predictors of a multiple regression can be measured by the variance inflation factor (VIF) (Fox and Monette, 1992). The high VIFs of 7.0 for surface sealing and 7.4 for built-up area confirm the high degree of collinear relationship. Since the surface sealing already includes built-up areas, as well as the other sealing structures, it serves as a cumulative factor for urbanization, which is suitable for city-scale analyses. It is assumed that the built-up area is already sufficiently represented by the surface sealing. Consequently, the less influential built-up area is removed from the further depth-oriented regression analysis. The correlation matrix further shows the absence of a high correlation between the remaining predictors (see Fig. 7). Furthermore, a low correlation among the local-scale predictors can be observed, due to the lack of spatial coincidence. As an example, there is no depth profile in the dataset where the district heating grid and a surface water is simultaneously upgradient of a measurement location. This was anticipated, since the surface waters with groundwater interaction lie exclusively near the northern border of the city where no district heating grid exists. Thus, the results reflect the spatial distribution of the local-scale factors, which does not negatively affect the regression results.

Table 2 shows the results of the initial multiple linear regression analysis of all large and local-scale factors studied. In detail, the z-scores are used with the mean temperature per depth profile to obtain the beta-coefficients, which allow us to compare influences and select dominant predictors for the depth-oriented analysis (cf. Section 2.4). There are already predictors within the dataset which cannot reach statistical significance, i.e. heating uses, surface waters and tunnels. In addition, sewers and metro stations exhibit a low significance. Among the significant predictors, surface sealing in particular shows the strongest positive influence, and saturated thickness the strongest negative one. They are followed by the district heating grid, built-up area, Darcy velocity and depth-to-water with considerable influences. As a result, the remaining predictors with minimal influence, i.e., cooling uses and deep buildings, sewers and metro stations are excluded from further depth-oriented analysis.

Fig. 8 displays the results of the depth-oriented multiple regression analysis with the five selected dominant factors. The x-axis shows the change of influence, i.e. the beta-coefficient, against the depth below ground for each factor. The depth of 2 mbgl is omitted, due to a low observation count (cf.

Table 2
Regression summary of the beta-coefficient estimation for all predictor variables with *t*-test and respective *p*-value.

Regression coefficient	Estimate	t value	Pr (>|t|)
Intercept	12.03	850.1	< 2e-16
Saturated groundwater thickness	−0.33	−20.0	< 2e-16
Depth-to-water	−0.13	−8.6	< 2e-16
Darcy velocity	−0.11	−6.9	< 2e-16
Cooling systems (injection wells)	−0.07	−4.6	5.1e-06
Heating systems (injection wells)	−0.02	−1.2	0.23
Surface waters with groundwater interaction	−0.02	−1.3	0.21
Surface sealing	0.93	24.9	< 2e-16
Built-up area	0.17	4.4	1.1e-05
Sewer system sections	0.03	1.8	0.07
Heating grid sections	0.17	11.8	< 2e-16
Deep buildings	−0.07	−4.6	4.4e-06
Metro stations	0.03	2.5	0.01
Tunnel sections	−0.001	−0.1	0.93

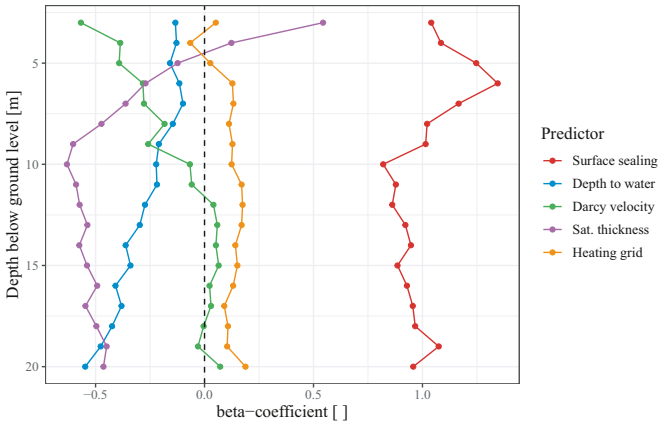

Fig. 8. Change of beta-coefficients against depth below ground for the dominant predictors.

Fig. 3a). First, it is noticeable that substantial vertical trends are only observable for cooling factors, whereas the influence of the surface sealing and the heating grid is relatively constant (cf. Fig. 8). The surface sealing maintains its very high driving influence on the groundwater temperature with the highest values around 5 mbgl to 7 mbgl. The heating grid shows a low but relatively continuous positive influence. In contrast, the cooling effect of depth-to-water is steadily increasing towards deeper levels and even surpasses the saturated thickness below 19 mbgl as dominant negative influence. For saturated thickness, the cooling effect increases until a depth of 10 mbgl and remains on a constant high negative influence in greater depths. The opposite behaviour can be observed for Darcy velocity. Its cooling effect steadily declines until it remains at around zero below depths of 10 mbgl. For all depth-dependent regressions, the beta-coefficients are statistically significant and the mean R^2 is 0.53 for depths above 10 mbgl, whereas it reaches 0.67 from 10 mbgl and below.

For a spatial visualisation of predictor influences, the dominant large-scale factors, i.e., surface sealing, depth-to-water, Darcy velocity and saturated thickness, are included in the thermal exposure score calculation. Fig. 9 presents the resulting grid, which indicates the exposure of the aquifer to the SSUHI (cf. Section 2.4). A positive score indicates that the dominant drivers prevail and the groundwater is subject to anthropogenic heating from surface sealing, whereas a negative score shows the dominance of cooling conditions from hydrogeological influences. The thermal exposure score has a Pearson correlation of 0.64 with the interpolated groundwater temperature. This already indicates how dominant large-scale factors contribute to the SSUHI and shows that local-scale factors are less significant on a city-wide scale. The temperatures displayed in Fig. 9 were measured one metre below groundwater level in April 2014 (cf. Section 2.2). Finally, the overlay pattern highlights the locally dominant factor resulting from the maximum product of the absolute beta-coefficient and z-score among the four predictors.

4. Discussion

The study developed a workflow based on exploratory data analysis for the evaluation of influences on the SSUHI in shallow aquifers. We applied a passive heat tracing procedure to estimate the weighted mean thermal diffusivity of the study area and successfully adjusted multi-temporal temperature measurements to a common seasonal state of a reference date. The large number of measurements analysed revealed that the sealing of the ground surface and built-up areas are the dominant drivers of anthropogenic groundwater warming in Munich. In addition, we showed that local-scale factors, like thermal groundwater uses, surface waters and underground structures do not have a significant influence on a city-wide scale. Moreover, we statistically elaborated how the magnitude of dominant influence changes with depth and thereby highlight the importance of the natural influence of saturated thickness, the Darcy velocity and the depth-to-water as major decreasing factors for groundwater warming. Finally, we calculated a thermal exposure score to display how the combined influence of large-scale influences matches the spatial groundwater temperature distribution and can therefore explain the SSUHI effect.

4.1. Discussion of the seasonal temperature influences

In the first step of the process, the classic additive approach proved its suitability by decomposing the 71 time series with minor residual variance in the random component. For this reason, the seasonal components derived serve as a resilient data basis for an extraction of time lag and amplitude. In addition, the dataset acquired covers the entire zone of seasonal fluctuation with a sufficient measurement density. The time-series dataset only lacks information from 1 mbgl to 4 mbgl, caused by the distribution of depth-to-water, as well as the common practice of installing temperature and pressure sensors near the bottom of observation wells. However, we could not observe a negative effect on the regression analyses. As verification, we calculated the Cook's distance, which is a measure of the influence of an observation on the regression result and takes leverage and residual into account (Cook, 1977). Based on its low Cook's distance (< 0.5), the measurement at 1 mbgl cannot be identified as an influential outlier, which indicates that the shallow area is already sufficiently represented. This observation is valid for both regression analyses (see Fig. 6).

In addition, it can be observed from Fig. 6 that the lag time and amplitude data has a residual variation, which cannot be explained by the fit of the regression equations. With the regression analysis, we derive the mean thermal diffusivity in the study area. Therefore, the residual variation originates mainly from different thermal diffusivities at the specific measurement sites. Since we assume the simplifications mentioned in Section 2.3, factors like a heterogeneous geology, the thickness of the unsaturated zone or the influence of other seasonal heat sources or sinks are not considered.

Furthermore, the differently high standard errors of the regression coefficients suggest that the estimated thermal diffusivities should be weighted according to their errors. Thus, we conducted the seasonal correction with the weighted mean thermal diffusivity. In comparison with the German VDI 4640–1, which states ranges of thermal conductivity and volumetric heat capacity, the resulting thermal diffusivity lies 65% above the typical characteristic value for saturated gravel and 29% above saturated sand. However, the thermal conductivity can vary considerably, with changing mineral composition and a total range of thermal diffusivity for saturated sand being given of between $0.59 \times 10^{-6}\, m^2 s^{-1}$ and $2.3 \times 10^{-6}\, m^2 s^{-1}$ (VDI, 4640). Therefore, the resulting averaged thermal diffusivity for the saturated sandy gravel of Munich ($1.24 \times 10^{-6}\, m^2 s^{-1}$) lies within a plausible range, although it is slightly elevated in comparison with typical characteristic values. Since Munich has a humid climate with a downward flow of infiltrated water in the vadose zone, a steady contribution by advective heat transport influences the groundwater when recharged. The enhanced heat transport as well as further convection in the groundwater body is not accounted for in the applied heat tracing method and elevated estimates are thus plausible. However, this deviation does not impair the statistical application in the correction procedure within the scope of this study, as the result integrates those effects through the least squares fit of the regression analysis (Kendall et al., 1983).

The same limitation is valid for the seasonal correction itself. Due to site specific influences, it may only be used in a statistical manner with a sufficient population size and not for adjusting individual temperature profiles. However, the statistical application showed that the seasonal effect has disappeared, which can be observed from comparing Fig. 3a and b. After the adjustment, the temperatures of all shallow depth levels show the same variance as the temperatures measured below 10 mbgl, i.e., approximately 3 °C. Thus, any bias in the regression analyses from different seasonal states has been successfully minimised.

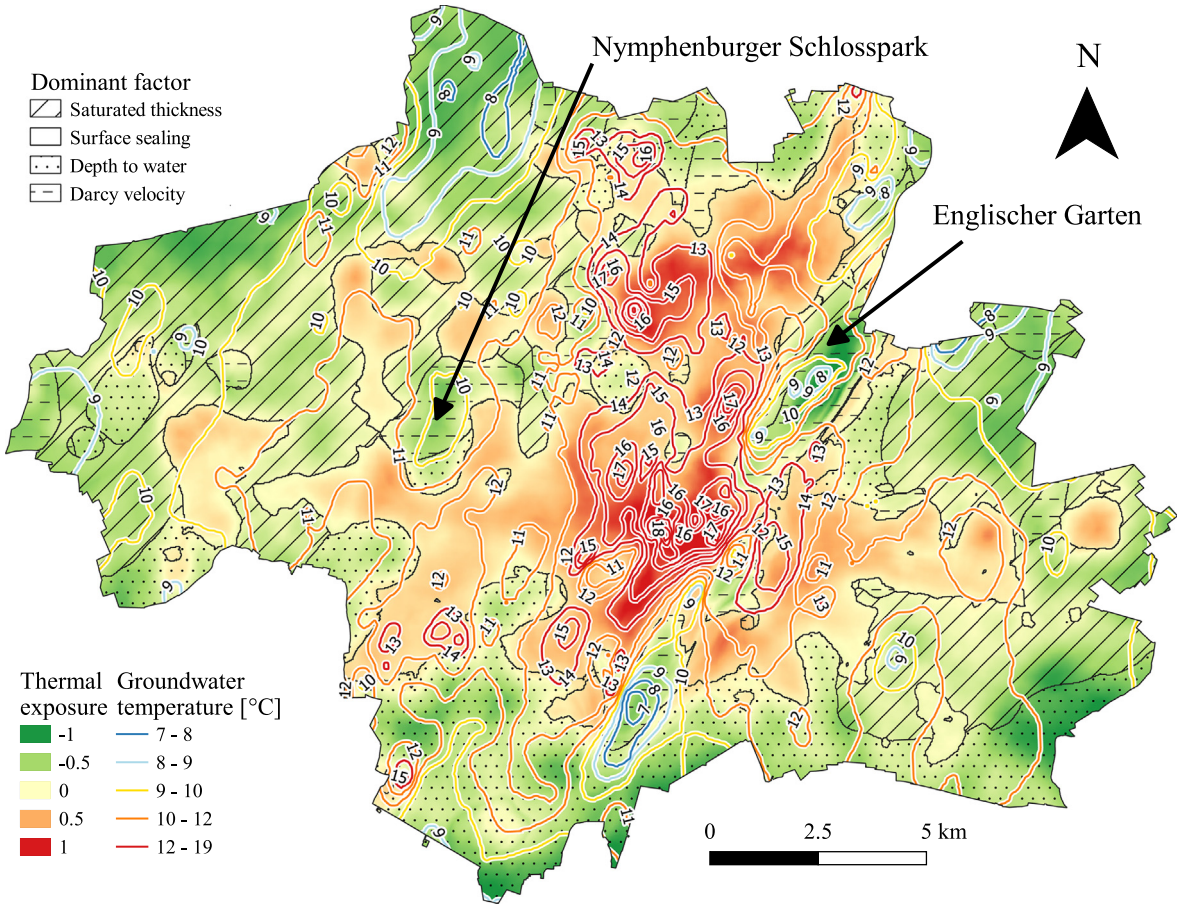

Fig. 9. Map of the thermal exposure score with an overlay pattern indicating the dominant factor in the score calculation and the contour lines of groundwater temperature interpolated from a reference date measurement in April 2014.

4.2. Discussion of the anthropogenic and natural influences

Prior to the regression analyses, the definition of the maximum influential area with triangular shapes revealed how spatial parameters differently affect the groundwater temperature. First, it can be stated that a single point value at the location of the measurement is generally not optimal for studying the dependency of a large-scale factor on groundwater temperature (cf. Fig. 5b). Consequently, in aquifers dominated by advective heat transport, any investigation that considers an up-gradient region with respect to the local groundwater flow direction will lead to stronger correlations because it reflects the advective transport processes. The possible gain in correlation strength will depend on the spatial variability of the factor. Since the hydrogeological parameters show less spatial heterogeneity than surface sealing and built-up area, the correlation coefficient also varies less (cf. Fig. 2). However, it can be concluded that the chosen procedure of considering the predictor values with the maximum correlation greatly affected the estimation and significance of regression coefficients and, therefore, improved the regression analyses.

Our findings in the initial comparative regression analysis are mostly in line with the interpretations of Dohr and Gruban (1999) and Zosseder (2015). Similar to many international SSUHI studies, we confirmed building density and surface sealing as major driving factors of subsurface warming in Munich (Taniguchi et al., 2005; Taniguchi et al., 2009; Yalcin and Yetemen, 2009; Epting and Huggenberger, 2013; Lokoshchenko and Korneva, 2015; Bucci, 2017; Marschalko et al., 2018; Visser et al., 2020). By using a novel surface sealing dataset, we were able to highlight the importance of green areas within the city to counteract the SSUHI effect. Most notably, this can be observed for the *Englischer Garten*, which lies Northeast of the city centre (cf. Fig. 9). In addition, surface sealing as a cumulative parameter for urban land use was superior to building footprints for the explanation of groundwater warming. Therefore, our results are consistent with the findings by Benz (2018) that in the absence of underground structures and basements, asphalt-covered land causes heat fluxes of a similar magnitude to buildings.

Furthermore, we proved the importance of hydrogeological factors for the temperature development of urban groundwater. As initially noticed by Zosseder (2015), areas with low saturated thickness can have naturally increased groundwater temperatures and may so potentially mask anthropogenic influences. A groundwater body with a higher saturated thickness can absorb more heat before the temperature increases, due to the larger water volume and the larger amount of advective heat transport. This leads to increased dispersion and consequently to the dissipation of higher temperatures. For that reason, our results indicate that advective heat transport constitutes the most important natural cause of higher or lower temperatures. Furthermore, the magnitude of advective heat transport is governed by the Darcy velocity. Hence, its influence is consistent with the anticipated cooling impact and confirms the plausibility and robustness of the regression estimation. The depth-to-water serves instead as an insulator between the surface and the groundwater body, due to the reduced thermal conductivity of the variably saturated zone with increasing air content. Thus, the regression estimate corresponds to its expected cooling influence, while the weak correlation with other factors verifies the absence of a negative spatial bias from the fact that the depth-to-water steadily decreases towards the north (cf. Fig. 1d). In conclusion, we emphasise that the natural conditions must be accounted for in future thermal evaluations of urban aquifers. Otherwise, naturally cooled or heated areas will not be identified,

climate-driven temperature changes will not be detected or perhaps wrongly classified as anthropogenic influenced (Epting and Huggenberger, 2013).

The comparative regression analysis of all predictors did not reveal a significant influence of thermal groundwater use for heating nor a positive influence for cooling, which is in line with Dohr and Gruban (1999). A warming influence of cooling systems and a cooling influence of heating systems would have been anticipated through direct advective inflow of thermally altered water (Stauffer et al., 2014). In part, the missing evidence for the impact of thermal uses can be explained by the measurement time. From April to June, the heating period is usually over and the domestic cooling period has - in most cases - not yet started. Therefore, thermal anomalies from small and medium-sized uses with a seasonal load profile could be already dissipated. Furthermore, larger cooling systems with relatively constant loads that might have a considerable local impact could not establish a warming influence on a city-wide scale. The small negative beta-coefficient for cooling systems can result from random residual noise in the temperature measurements which was attributed to the variation of this factor and can, therefore not be linked to a causal reason. However, we can conclude that the thermal use of groundwater had no considerable influence on the city-wide groundwater temperature of Munich over the measurement period.

In agreement with Dohr and Gruban (1999), we did not observe a significant influence of the sewers. In general, the sewers should contribute to groundwater warming as buildings discharge 15% - 30% of their supplied thermal energy through the sewer system (Schmid, 2008). Thus, the sewer pipes act as a heat carrier, which dissipates heat into the ground mainly through conduction (Frijns et al., 2013; Stauffer et al., 2014). However, also advective heat inflow into the ground can happen through leakage in the pipes. Since waste heat in the mostly shallow sewers is relatively warmer than the ground in winter, its potentially warming impact will be more observable in late winter or early spring (Cipolla and Maglionico, 2014).

In contrast to thermal uses and the sewer system, the heating grid influences the underground only through conductive heat transfer into the ground (Sami and Maltais, 2000; Çomakli et al., 2004; Stauffer et al., 2014). Leakage is rare and in the case of an event only temporary, due to a constant monitoring. Following the indirect observation of Dohr and Gruban (1999), we were able to identify a small influence of the heating grid. This finding is in line with Benz (2015) and Tissen et al. (2019), however, a differentiation must be made between Munich's modern heating grid and the older steam grid with a higher supply temperature. Thus, we suggest reviewing the influence of the heating grid in the future to gain a clearer view of the underlying dependencies.

Contrary to the suggestions by Dohr (1989, 2011), no particular warming effect from large subsurface buildings, underground stations and metro tunnels could be proven on city scale. In the local surroundings of metro tunnels, the depth profile measurements show 2 °C to 3 °C higher temperatures compared to up-gradient temperatures. The groundwater temperature anomalies, however, mostly dissipate at distances of more than 10 m – an observation that is also anticipated for subsurface building structures. A detailed distribution of groundwater temperatures grouped by distance to metro tunnels is provided as supplementary material (cf. SI: Fig. 2). Locally, our observations are comparable with the thermal impact of underground parking lots studied by Becker and Epting (2021), where the seasonal evaluation also showed that a warming influence is generally the lowest in spring. The study additionally observed that the thermal impact of freeway tunnels is highly seasonal, i.e. a cooling influence in late winter and spring and a warming influence in late summer and autumn. Therefore, the absence of a city-wide warming influence of subsurface buildings and tunnels can also result from the high dependence on usage and seasonality. Epting et al. (2017) has highlighted that tracking the diffuse conductive thermal impact of subsurface building structures by down-gradient temperature measurements is challenging. Due to the city-wide investigation, the locally observed influences might be largely overshadowed by the dominant spatial factors; local warming would also be more intense in winter (Dohr, 1989).

Lastly the regression analysis could not establish a significant influence by surface waters on the groundwater temperature. In general, a cooling influence from surface waters would be expected as relatively cooler lake water infiltrates into the aquifer during the winter and spring months. This cold plume moves down-gradient through advective heat transport and should still be observable in measurements made from May to June (Anderson, 2005). However, since surface waters with substantial groundwater infiltration are only located on the northern border of the study area, most measurement wells are not influenced by them and, consequently, little influence was anticipated. In addition, it must be noted that the influence of the river *Isar* was outside the scope of this study, because the river is mostly the receiving water and river water infiltration commonly influences the narrow surroundings of the river bed.

In summary, the comparative analysis provided conclusive information for the selection of dominant predictors. Hence, the following depth-dependent examination could reveal novel insights on the change of influences in the shallow gravel aquifer of Munich. Initially, the driving influences observed do not decline with depth, which supports the approach of SSUHI studies covering influences below the seasonal fluctuation zone (Ferguson and Woodbury, 2004; Reiter, 2007; Menberg et al., 2013b; Benz, 2018; Hemmerle et al., 2019). However, the influences of hydrogeological factors show greater variability with depth. In part, this behaviour can be attributed to the different heat transport mechanisms described above. For the Darcy velocity, the results indicate that the magnitude of dispersive mixing is most relevant near the surface. At shallow depths, higher temperature gradients are present, which dissipate faster than lower gradients. Therefore, the Darcy velocity becomes less relevant in deeper sections of the aquifer, i.e., below 10 mbgl, where higher temperature gradients are no longer present.

In the depth-dependent analyses of saturated thickness and depth-to-water, however, spatial implications must also be considered. The deeper groundwater temperatures are measured, the larger the possible depth-to-water and the higher the chance that the measurement will be made in a lower section of the aquifer. An increasing depth-to-water steadily increases the insulating effect and thus, the influence also grows continuously. A similar dependency can be observed for saturated thickness. With greater depth, the volume of water that needs to be heated increases, and at the same time the greater volume offers space for horizontal advective heat transport. Consequently, the possible cooling effect of saturated thickness also increases.

Finally, an appropriate basis for the spatial evaluation of thermal influences on an urban aquifer is introduced by the thermal exposure mapping (see Fig. 9). The results explain the origin of specific temperature patterns in the groundwater and reveal a strong interaction with the surface. As a shown in Fig. 1e, we observe a compartmentalised SSUHI below Munich similar to the description of the UHI (Funk et al., 2014). Large parks like the *Englischer Garten* and the *Nymphenburger Schlosspark* are responsible for a substantial cooling of the groundwater (cf. Figs. 1e and 9). However, the cooling influence of intermediate sized parks is also evident near the city centre (cf. SI: Fig. 1). In addition, it must be noted that the groundwater temperatures in April 2014 still reflected different seasonal conditions, because they were measured 1 m below groundwater level. As it is visible in Fig. 1d, the depths-to-water in the northern, north-eastern and north-western parts of the city are lower than in the south. Therefore, these shallower measurements have a tendency towards lower temperatures, especially in April when the seasonal temperatures at depths from 2 mbgl to 6 mbgl are among the lowest of the year (see Fig. 3a). Despite this characteristic, a reasonably strong correlation between the exposure score and the interpolated groundwater temperature provides further verification of the significance of the dependencies derived throughout the entire study area.

5. Conclusions

Urban environmental authorities nowadays implement sophisticated strategies to reduce greenhouse gas emissions and to protect valuable natural resources. Urban groundwater bodies in particular are subject to warming, which can threaten groundwater quality. However, for groundwater, the development of policies is not straightforward, since there is a conflict between the priorities of thermal use and groundwater protection.

It is therefore crucial to understand the dependency and importance of each influential factor before city-wide groundwater protection strategies can be drafted. With this paper, we offer a resilient and comprehensive assessment of the anthropogenic and natural factors that have a significant influence on the groundwater temperature in the shallow aquifer of Munich. A database of temperature time series, depth profiles and a variety of high-resolution spatial datasets allowed the statistical analysis of a depth-dependent change in influence among the dominant factors.

Based on our results, we suggest that often neglected hydrogeological factors should be considered in studies on the SSUHI effect, since they play a key role as mitigating factors. Furthermore, the adjustment of multi-temporal measurements within the zone of seasonal fluctuation delivered appropriate results and is applicable to similar shallow urban aquifers if time series data is available. Finally, the influences identified deliver valuable information on the parametrisation and definition of boundary conditions in numerical models. Above all, the surface temperature boundary condition in shallow aquifers has a key influence on the simulation of thermal anomalies.

Concerning future groundwater monitoring networks, it becomes visible how important it is to capture the temporal dynamic and a vertical resolution. In addition, a monitoring network should be spatially balanced. Since measurements are often carried out to observe the impact of specific point sources, the interpretation on a city-scale can be biased. The outcome that thermal uses and specific underground structures, like sewers, tunnels and deep basements, cannot establish a city-wide significant influence, whereas sealing and built-up areas that have a strong influence on groundwater warming can help to establish measures for mitigating elevated urban groundwater temperatures. Hence, the debate about preserving the thermal conditions of the groundwater should focus more on dealing with large-scale factors and integrating this aspect into urban planning. For instance, the Sponge City Concept could help mitigate groundwater warming in cities (Zevenbergen et al., 2018).

CRediT authorship contribution statement

Fabian Böttcher: Conceptualization, Methodology, Formal analysis, Data Curation, Writing, Visualization **Kai Zosseder:** Conceptualization, Review & Editing, Supervision, Funding acquisition.

Declaration of competing interest

The authors declare that they have no known competing financial interests or personal relationships that could have appeared to influence the work reported in this paper.

Acknowledgements

The financial support for this research within the Geo.KW project by the Federal Ministry for Economic Affairs and Energy (BMWi) under Grant Number 03ETW004A is gratefully acknowledged. Further, we thank Patrick Kotyla, Teresa Zölch (Referat für Klima und Umweltschutz), Immanuel Pache (Stadtwerke München) and Tobias Leichtle (Deutsches Zentrum für Luft- und Raumfahrt) for their valuable and essential support with data and additional information.

Appendix A. Supplementary data

Supplementary data to this article can be found online at https://doi.org/10.1016/j.scitotenv.2021.152193.

References

Agudelo-Vera, C., et al., 2020. Drinking water temperature around the globe: understanding, policies, challenges and opportunities. Water (Switzerland) 12 (4), 1–19. https://doi.org/10.3390/W12041049.

Albarrán-Ordás, A., Zosseder, K., 2020. 'Geostatistische Reliefmodellierung der quartären Grundwasserleiterbasis in der Münchener Schotterebene unter Verwendung von Massendaten', Zeitschrift der Deutschen Gesellschaft für Geowissenschaften. 171(1). Schweizerbart Science Publishers, Stuttgart, Germany, pp. 1–19. https://doi.org/10.1127/zdgg/2020/0206.

Allen, A., Milenic, D., Sikora, P., 2003. Shallow gravel aquifers and the urban "heat island" effect: a source of low enthalpy geothermal energy. Geothermics 32 (4), 569–578. https://doi.org/10.1016/S0375-6505(03)00063-4.

Anderson, M.P., 2005. Heat as a ground water tracer. Ground Water 43 (6), 951–968. https://doi.org/10.1111/j.1745-6584.2005.00052.x.

Banks, D., 2009. An introduction to "thermogeology" and the exploitation of ground source heat. Q. J. Eng. Geol. Hydrogeol. 42 (3), 283–293. https://doi.org/10.1144/1470-9236/08-077.

Banks, D., 2012. An Introduction to Thermogeology: Ground Source Heating And Cooling. 2nd edn. Wiley-Blackwell, Oxford.

Becker, D., Epting, J., 2021. Thermal impact of subsurface urban structures on groundwater temperatures in the city of Basel. Grundwasser 26 (3), 269–288. https://doi.org/10.1007/s00767-021-00483-1.

Benz, S.A., 2015. Spatial resolution of anthropogenic heat fluxes into urban aquifers. Science of the Total Environment. 524–525. Elsevier B.V., pp. 427–439. https://doi.org/10.1016/j.scitotenv.2015.04.003.

Benz, S.A., 2018. Comparing anthropogenic heat input and heat accumulation in the subsurface of Osaka, Japan. Science of the Total Environment. Elsevier B.V. 643, pp. 1127–1136. https://doi.org/10.1016/j.scitotenv.2018.06.253.

Benz, S.A., et al., 2016. Linking surface urban heat islands with groundwater temperatures. Environ. Sci. Technol. 50 (1), 70–78. https://doi.org/10.1021/acs.est.5b03672.

Benz, S.A., Bayer, P., Blum, P., 2017. Identifying anthropogenic anomalies in air, surface and groundwater temperatures in Germany. Science of the Total Environment. 584–585. Elsevier B.V., pp. 145–153. https://doi.org/10.1016/j.scitotenv.2017.01.139.

Bidarmaghz, A., 2019. Influence of geology and hydrogeology on heat rejection from residential basements in urban areas. Tunnelling and Underground Space Technology. 92(August). Elsevier, p. 103068. https://doi.org/10.1016/j.tust.2019.103068.

Blum, P., et al., 2010. CO2 savings of ground source heat pump systems - a regional analysis. Renew. Energy 35 (1), 122–127. https://doi.org/10.1016/j.renene.2009.03.034.

Bonte, M., van Breukelen, B.M., Stuyfzand, P.J., 2013. Temperature-induced impacts on groundwater quality and arsenic mobility in anoxic aquifer sediments used for both drinking water and shallow geothermal energy production. Water Research. 47(14). Elsevier Ltd, pp. 5088–5100. https://doi.org/10.1016/j.watres.2013.05.049.

Böttcher, F., et al., 2019. TAP - thermal aquifer potential: a quantitative method to assess the spatial potential for the thermal use of groundwater. Renew. Energy 142 (April). https://doi.org/10.1016/j.renene.2019.04.086.

Brielmann, H., et al., 2009. Effects of thermal energy discharge on shallow groundwater ecosystems. FEMS Microbiol. Ecol. 68 (3), 273–286. https://doi.org/10.1111/j.1574-6941.2009.00674.x.

Bucci, A., 2017. Shallow groundwater temperature in the Turin area (NW Italy): vertical distribution and anthropogenic effects. Environmental Earth Sciences. 76(5. Springer Berlin Heidelberg. https://doi.org/10.1007/s12665-017-6546-4.

Carslow, H.S., Jaeger, J.C., Morral, J.E., 1986. Conduction of heat in solids. Journal of Engineering Materials and Technology, 2nd edn. Clarendon Press, Oxford https://doi.org/10.1115/1.3225900 (2nd edn.).

Cipolla, S.S., Maglionico, M., 2014. Heat recovery from urban wastewater: analysis of the variability of flow rate and temperature. Energy and Buildings. 69. Elsevier B.V., pp. 122–130. https://doi.org/10.1016/j.enbuild.2013.10.017.

Çomakli, K., Yüksel, B., Çomakli, Ö., 2004. Evaluation of energy and exergy losses in district heating network. Appl. Therm. Eng. 24 (7), 1009–1017. https://doi.org/10.1016/j.applthermaleng.2003.11.014.

Cook, R.D., 1977. Detection of influential observations in linear regression. Technometrics 22, 494–508.

Dohr, F., 1989. Die Grundwassertemperatur im oberflächennahen Grundwasser des Stadtgebiets München. Ludwig-Maximilians-Universität.

Dohr, F., 2011. Grundwassertemperaturen München: Messungen 2009 - 2010 München.

Dohr, F., Gruban, W., 1999. Überwachungssystem der Landeshauptstadt München München.

Eggleston, J., McCoy, K.J., 2015. Assessing the magnitude and timing of anthropogenic warming of a shallow aquifer: example from Virginia Beach, USA. Hydrogeol. J. 23 (1), 105–120. https://doi.org/10.1007/s10040-014-1189-y.

Epting, J., Huggenberger, P., 2013. Unraveling the heat island effect observed in urban groundwater bodies - definition of a potential natural state. Journal of Hydrology. 501. Elsevier B.V., pp. 193–204. https://doi.org/10.1016/j.jhydrol.2013.08.002.

Epting, J., Händel, F., Huggenberger, P., 2013. Thermal management of an unconsolidated shallow urban groundwater body. Hydrol. Earth Syst. Sci. 17 (5), 1851–1869. https://doi.org/10.5194/hess-17-1851-2013.

Epting, J., et al., 2017. The thermal impact of subsurface building structures on urban groundwater resources – a paradigmatic example. Science of the Total Environment. 596–597. Elsevier B.V., pp. 87–96. https://doi.org/10.1016/j.scitotenv.2017.03.296.

Everitt, B., Hothorn, T.J., 2011. An Introduction to Applied Multivariate Analysis With R. Springer, New York https://doi.org/10.1007/978-1-4419-9650-3.

Farr, G.J., et al., 2017. Mapping shallow urban groundwater temperatures, a case study from Cardiff, UK. Q. J. Eng. Geol. Hydrogeol. 50 (2), 187–198. https://doi.org/10.1144/qjegh2016-058.

Ferguson, G., Woodbury, A.D., 2004. Subsurface heat flow in an urban environment. J. Geophys. Res. Solid Earth 109 (B2). https://doi.org/10.1029/2003JB002715 (pp. B02402–B02402).

Ferguson, G., Woodbury, A.D., 2007. Urban heat island in the subsurface. Geophys. Res. Lett. 34 (23), 2–5. https://doi.org/10.1029/2007GL032324.

Fox, J., Monette, G., 1992. Generalized collinearity diagnostics. Journal of the American Statistical Association. 87(417). Taylor & Francis Group, pp. 178–183. https://doi.org/10.1080/01621459.1992.10475190.

Frijns, J., Hofman, J., Nederlof, M., 2013. The potential of (waste)water as energy carrier. Energy Conversion and Management. 65. Elsevier Ltd, pp. 357–363. https://doi.org/10.1016/j.enconman.2012.08.023.

Funk, D., Groß, G., Trute, P., 2014. Stadtklimaanalyse Landeshauptstadt München, Landeshauptstadt München - Referat für Gesundheit und Umwelt. Munich.
García-Gil, A., et al., 2018. Decreased waterborne pathogenic bacteria in an urban aquifer related to intense shallow geothermal exploitation. Science of the Total Environment. 633. Elsevier B.V., pp. 765–775. https://doi.org/10.1016/j.scitotenv.2018.03.245.
Goto, S., 2005. Thermal response of sediment with vertical fluid flow to periodic temperature variation at the surface. J. Geophys. Res. 110 (B1), B01106. https://doi.org/10.1029/2004JB003419.
Greenland, S., et al., 1991. Standardized regression coefficients. Epidemiology 2 (5), 387–392. https://doi.org/10.1097/00001648-199109000-00015.
Gunawardhana, L.N., Kazama, S., Kawagoe, S., 2011. Impact of urbanization and climate change on aquifer thermal regimes. Water Resour. Manag. 25 (13), 3247–3276. https://doi.org/10.1007/s11269-011-9854-6.
Hatch, C.E., et al., 2006. Quantifying surface water-groundwater interactions using time series analysis of streambed thermal records: method development. (p. n/a–n/a)Water Resour. Res. 42 (10). https://doi.org/10.1029/2005WR004787.
Hemmerle, H., et al., 2019. Estimation of groundwater temperatures in Paris, France. Geofluids. Wiley Hindawi, p. 11 https://doi.org/10.1155/2019/5246307.
Jerz, H., 1993. Geologie von Bayern II - Das Eiszeitalter in Bayern: Erdgeschichte, Gesteine, Wasser, Boden. Stuttgart: E. Schweizerbart'sche Verlagsbuchhandlung.
Jesußek, A., Grandel, S., Dahmke, A., 2013. Impacts of subsurface heat storage on aquifer hydrogeochemistry. Environ. Earth Sci. 69 (6), 1999–2012. https://doi.org/10.1007/s12665-012-2037-9.
Keery, J., et al., 2007. Temporal and spatial variability of groundwater–surface water fluxes: development and application of an analytical method using temperature time series. J. Hydrol. 336 (1–2), 1–16. https://doi.org/10.1016/j.jhydrol.2006.12.003.
Kendall, M., Stuart, A., Ord, J.K., 1983. The Advanced Theory of Statistics. 4th edn. Vol. 3. Charles Griffin and Co., Ltd., London, GB.
Kerl, M., et al., 2012. Hydrogeologisches Konzeptmodell von München: Grundlage für die thermische Grundwassernutzung. Grundwasser 17 (3), 127–135. https://doi.org/10.1007/s00767-012-0199-8.
Konikow, L.F., Bredehoeft, J.D., 1984. Computer model of two-dimensional solute transport and dispersion in ground water. Techniques of Water-resources Investigations. 7(2). United States Geological Survey, p. 90.
Leichtle, T., Martin, K., Taubenböck, H., 2018. On the capability of optical remote sensing imagery with various spatial resolutions on impervious surface estimation. EARSeL 5th Joint Workshop "Urban Remote Sensing – Challenges & Solutions".
Lemcke, K., 1988. Geologie von Bayern I - Das bayerische Alpenvorland vor der Eiszeit. Stuttgart: E. Schweizerbart'sche Verlagsbuchhandlung.
Li, X., 2019. Urban heat island impacts on building energy consumption: a review of approaches and findings. Energy. 174. Elsevier Ltd, pp. 407–419. https://doi.org/10.1016/j.energy.2019.02.183.
Lokoshchenko, M.A., Korneva, I.A., 2015. Underground urban heat island below Moscow city. Urban Climate. 13. Elsevier B.V., pp. 1–13. https://doi.org/10.1016/j.uclim.2015.04.002.
Marschalko, M., et al., 2018. Heat contamination in groundwater sourced from heat pump for heating in Bratislava (Slovakia)'s historic centre. Environmental Earth Sciences. 77(3). Springer Berlin Heidelberg, pp. 1–12. https://doi.org/10.1007/s12665-018-7284-y.
Menard, S., 2004. Standardized regression coefficients. In: Lewis-Beck, M.S., Bryman, A., Liao, T.F. (Eds.), The Sage Encyclopedia of Social Science Research Methods. Sage Publications, Thousand Oaks, CA, USA, pp. 1069–1070.
Menberg, K., Blum, P., et al., 2013. Long-term evolution of anthropogenic heat fluxes into a subsurface urban heat island. Environ. Sci. Technol. 47 (17), 9747–9755. https://doi.org/10.1021/es401546u.
Menberg, K., Bayer, P., et al., 2013. Subsurface urban heat islands in German cities. Science of the Total Environment. 442. Elsevier B.V., pp. 123–133. https://doi.org/10.1016/j.scitotenv.2012.10.043.
Molina-Giraldo, N., et al., 2011. Propagation of seasonal temperature signals into an aquifer upon bank infiltration. Ground Water 49 (4), 491–502. https://doi.org/10.1111/j.1745-6584.2010.00745.x.
Mühlbacher, G., 2020. Stadtklimatische Untersuchungen der sommerlichen Temperaturverhältnisse und des Tagesgangs des Regionalwindes („Alpines Pumpen") in München. Offenbach am Main.
Müller, N., Kuttler, W., Barlag, A.B., 2014. Analysis of the subsurface urban heat island in Oberhausen, Germany. Clim. Res. 58 (3), 247–256. https://doi.org/10.3354/cr01195.
Oke, T.R., 1982. The energetic basis of the urban heat island. Q. J. R. Meteorol. Soc. 108 (455), 1–24.
Oke, T.R., et al., 2017. Urban Climates. Cambridge University Press, Cambridge https://doi.org/10.1017/9781139016476.
OpenStreetMap contributors, 2021. Planet dump. retrieved from https://planet.osm.org.
Peel, M.C., Finlayson, B.L., McMahon, T.A., 2007. Updated world map of the Köppen-Geiger climate classification. Hydrol. Earth Syst. Sci. 11, 1633–1644. https://doi.org/10.5194/hess-11-1633-2007.
Reiter, M., 2007. Variability of recent ground surface temperature changes in the Albuquerque basin, central New Mexico. J. Geophys. Res. Atmos. 112 (24), 1–9. https://doi.org/10.1029/2006JD008215.
Rivera, J.A., Blum, P., Bayer, P., 2017. Increased ground temperatures in urban areas: estimation of the technical geothermal potential. Renewable Energy. 103. Elsevier Ltd, pp. 388–400. https://doi.org/10.1016/j.renene.2016.11.005.
van Ruijven, B.J., De Cian, E., Sue Wing, I., 2019. Amplification of future energy demand growth due to climate change. Nature Communications. 10(1). Springer, US, pp. 1–12. https://doi.org/10.1038/s41467-019-10399-3.
Sami, S.M., Maltais, H., 2000. On transient heat losses from buried district heating pipes. Int. J. Energy Res. 24 (15), 1311–1334. https://doi.org/10.1002/1099-114X(200012)24:15<1311::AID-ER648>3.0.CO;2-Q.
Schielzeth, H., 2010. Simple means to improve the interpretability of regression coefficients. Methods Ecol. Evol. 1 (2), 103–113. https://doi.org/10.1111/j.2041-210x.2010.00012.x.
Schmid, F., 2008. Sewage water: interesting heat source for heat pumps and chillers. Available at9th International IEA Heat Pump Conference, 20–22 May 2008, Zürich, Switzerland, (May) , pp. 1–12. https://heatpumpingtechnologies.org/publications/sewage-water-interesting-heat-source-forheat-pumps-and-chillers/.
Stallman, R.W., 1965. Steady one-dimensional fluid flow in a semi-infinite porous medium with sinusoidal surface temperature. J. Geophys. Res. 70 (12), 2821–2827. https://doi.org/10.1029/jz070i012p02821.
Stauffer, F., et al., 2014. Thermal Use of Shallow Groundwater. Taylor & Francis Group, Boca Raton.
Taniguchi, M., Uemura, T., Sakura, Y., 2005. Effects of urbanization and groundwater flow on subsurface temperature in three megacities in Japan. J. Geophys. Eng. 2 (4), 320–325. https://doi.org/10.1088/1742-2132/2/4/S04.
Taniguchi, M., Uemura, T., Jago-on, K., 2007. Combined effects of urbanization and global warming on subsurface temperature in four Asian cities. Vadose Zone J. 6 (3), 591–596. https://doi.org/10.2136/vzj2006.0094.
Taniguchi, M., et al., 2009. Anthropogenic effects on the subsurface thermal and groundwater environments in Osaka, Japan and Bangkok, Thailand. Science of the Total Environment. 407(9). Elsevier B.V., pp. 3153–3164. https://doi.org/10.1016/j.scitotenv.2008.06.064.
Tauxe, J.D., 1994. Porous Medium Advection-dispersion Modeling in a Geographic Information System, Center for Research in Water Resources. University of Texas at Austin.
Theel, M., Huggenberger, P., Zosseder, K., 2020. Assessment of the heterogeneity of hydraulic properties in gravelly outwash plains: a regionally scaled sedimentological analysis in the Munich gravel plain, Germany. Hydrogeol. J. 28 (8), 2657–2674. https://doi.org/10.1007/s10040-020-02205-y.
Thomson, W., 1861. On the reduction of observations of underground temperature. Trans. R. Soc. Edinburgh 22 (2), 405–427.
Tissen, C., et al., 2019. Groundwater temperature anomalies in central Europe. Environmental Research Letters. 14(10). IOP Publishing. https://doi.org/10.1088/1748-9326/ab4240.
Van Wijk, W.R., de Vries, D.A., 1963. Thermal properties of soils. In: Van Wijk, W.R. (Ed.), Physics of Plant Environment, 2nd edn. North-Holland Publishing Company, Amsterdam, pp. 210–235.
VDI (4640) 'Richtlinie 4640, 2000. Thermal use of the ground. Fundamentals, Approvals, Environmental Aspects. Verein Deutscher Ingenieure, Part 1. Beuth Verlag GmbH.
Venables, W.N., Ripley, B.D., 2002. Modern Applied Statistics With S. 4th edn. Springer-Verlag, Heidelberg https://doi.org/10.1214/aoms/1177697510.
Visser, P.W., et al., 2020. Impacts of progressive urban expansion on subsurface temperatures in the city of Amsterdam (The Netherlands). Hydrogeol. J. 28 (5), 1755–1772. https://doi.org/10.1007/s10040-020-02150-w.
Wurm, M., et al., 2011. Object-based image information fusion using multisensor earth observation data over urban areas. Int. J. Image Data Fusion 2 (2), 121–147. https://doi.org/10.1080/19479832.2010.543934.
Yalcin, T., Yetemen, O., 2009. Local warming of groundwaters caused by the urban heat island effect in Istanbul, Turkey. Hydrogeol. J. 17 (5), 1247–1255. https://doi.org/10.1007/s10040-009-0474-7.
Zevenbergen, C., Fu, D., Pathirana, A., 2018. Transitioning to sponge cities: challenges and opportunities to address urban water problems in China. Water (Switzerland) 10 (9), 13. https://doi.org/10.3390/w10091230.
Zhu, K., et al., 2010. The geothermal potential of urban heat islands. Environ. Res. Lett. 5 (4), 6. https://doi.org/10.1088/1748-9326/5/4/044002.
Zhu, K., et al., 2015. Groundwater temperature evolution in the subsurface urban heat island of Cologne, Germany. Hydrol. Process. 29 (6), 965–978. https://doi.org/10.1002/hyp.10209.
Zosseder, K., 2007. Heterogene Verteilung von PAK-Kontaminationen im Grundwasser', Bochumer Geowissenschaftliche Arbeiten. 12, p. 236.
Zosseder, K., 2013. GEPO – Geothermisches Potenzial der Münchener Schotterebene Abschätzung des geothermischen Potenzials im oberflächennahen Unter- grund des quartären Grundwasserleiters des Großraum Münchens .', in 19. Tagung für Ingenieurgeologie. München, pp. 265–270.
Zosseder, K., 2015. Abschlussbericht zum Forschungsvorhaben: 'Erstellung einer Datengrundlage für die Abschätzung des geothermischen Potenzials im oberflächennahen Untergrund des quartären Grundwasserleiters des Großraum Münchens'. München.